Title Large Earthquakes: a Way of Formation and Prediction

Author Zhiyong ZHU

Affiliation Shanghai Institute of Applied Physics, Chinese Academy of Science

E-mail zhuzhiyong@sinap.ac.cn

Large Earthquakes: a Way of Formation and Prediction

Zhiyong ZHU*

Shanghai Institute of Applied Physics, Chinese Academy of Science

Jialuo Rd.2019, 201800, Shanghai, P. R. China

E-mail: zhuzhiyong@sinap.ac.cn

Abstract

It is believed that the accumulation of small fractures (small earthquakes) in the crust is one of many ways for the formation of large fractures (large earthquakes). In such cases, the temporal variations in the accumulation number of small earthquakes can be used to predict future seismic activity in the region. To do so, a structural system of the crust is constructed using the logarithmic linear relationship between earthquake frequency and magnitude, and a relationship between earthquake accumulation and time is derived by assuming that the rate of earthquake accumulation is proportional to the q-th power of the existing number of earthquakes. Earthquake record from selected regions of China and Italy are fitted by the theory and the obtained fitting parameters are used to evaluate the future seismic activity. It is found that the extent of deviation of earthquake accumulation from the theoretical expectation can be a reasonable judgement of the local seismic dangerous level and $q \geq 1$ can be considered a marker of local crust entering an accelerated fracturing phase. The proposed method made the physical evaluation of local seismic activity possible by simplifying the 3D (space-time-magnitude) problem into 2D (time-magnitude) problem in earthquake prediction.

Keywords: Earthquake prediction, Seismic activity, Precursor, Self-organized critical processes

1. Introduction

Earthquake could be the severest disaster faced by humanity with about 54% deaths caused over all natural disasters [1, 2]. The exploration of earthquakes has a long history, with modern scientific research beginning in the late 19th century. Although great progress has been achieved with continuous improvements in detection technology and the development of theoretical analysis methods [3-5] in the past 100 years, we remain still far from achieving the goal of earthquake prediction [5, 6]. Scientists have expressed skepticism about the possibility of earthquake prediction from time to time, and even come into a heated argument on this issue in the late 20th century [7-11].

The key points of the debate focus on two aspects. The first is whether earthquake precursors exist? How should earthquake precursors be defined and identified, and what is their physical basis?

* Corresponding author: Zhiyong ZHU (E-mail: zhuzhiyong@sinap.ac.cn)

The second is whether earthquakes are self-organized critical (or near-critical) processes? Are earthquakes inherently random? Discussions on the first type of question have generated many constructive insights, which have helped standardize future screening and identification of earthquake precursors [4]. However, there is no consensus on the second type of question. Some argue that the self-organized critical nature of earthquakes determines their randomness, suggesting that any small geological process could trigger a major earthquake [7, 11]. Others deny the randomness of earthquakes, asserting that the crust is not always in a self-organized critical state, and that chaotic and nonlinear phenomena mainly occur during the unstable sliding phase [12]. Furthermore, they argue that this self-organized critical state can itself be considered a precursor to earthquakes. While debates continue, the scientific community generally agrees that without a reliable fundamental theory of earthquakes it will be difficult to provide prediction services for society. Due to the difficulties in detecting geological structures deep underground, earthquake research has largely relied on a hypothesis-to-verification approach, gradually approaching the truth through the process of eliminating improper hypotheses.

The present work believes that accumulation of small fractures (small earthquakes) over years in the crust is one of the way for the formation of large fractures (large earthquakes). It is also proposed that crustal structures, like other materials, are organized systems where smaller structures form larger structures, and larger structures form even larger ones. The so-called logarithmic linear relationship between earthquake frequency and magnitude is merely an outward manifestation of the structural composition of materials under external forces. Based on these propositions, a theoretical relationship for the evolution of small earthquakes into large earthquakes has been derived, and is used to analyze earthquake data (here referring to the accumulation of earthquake occurrence numbers over time, the same below) from selected regions. The results show that the accumulation of small earthquakes in certain regions can reflect the crustal energy level of local region, and the temporal change in small earthquake frequency can be used to judge future regional seismic activity.

2. Basic considerations

Earthquakes (here referring to tectonic earthquakes, the same below) are caused by fractures of crust resulting in rapid displacement between tectonic plates or crust blocks. It is generally believed that crustal fractures occur when compressive forces between tectonic plates exceed their local fracture strength [13]. This explanation accounts for earthquakes caused by compression and collision along plate boundaries. However, the source of forces driving earthquakes in inland regions far from plate boundaries remains uncertain. Considering that the Earth is an approximately spherical structure with a solid crust enveloping a fluid-like mantle [14], the Earth's rotation and its periodic orbital motion around the Sun inevitably subject the crust to long-term periodic impacts from the mantle. These impacts can be directly generated by mantle dynamics, or indirectly resulting from mantle-induced stress transfer. Such impacts are analogous to the forces exerted on the inner walls of a rotating cement mixer by the cement inside. The fact that mountainous areas on the Earth's surface are more prone to earthquakes than plains support the proposition since the inner surface of the crust corresponding to mountainous area are structures protruding inward that would be more susceptible to mantle impacts compared to flatter regions. Given the long-term stability of Earth's structure and

orbital motion, it can be considered that this impact stress is stable and with a fixed amplitude for each region.

The periodic tidal fluctuations of the oceans can exert impact forces along ocean-land boundaries and therefore may potentially producing similar effect. Even if the stress intensity of such impacts is not high enough, the continuous and repetitive nature of these forces over long periods can still cause damage to crustal structures, creating conditions for the downward migration of crustal material under the influence of gravity. In other words, periodic impacts caused by the mantle result in the destruction of crustal structures. The destruction of these structures allows the crust to fracture and move under gravitational forces. The rapid relative movement between fractured crustal sections generates earthquakes with magnitudes corresponding to the fractured size. This process is similar to a high-rise building collapsing after its foundational structure is gradually damaged. The collapse causes ground vibrations while enabling the transfer of material from regions of high gravitational potential to regions of low gravitational potential.

Of course, the apparent mechanical mechanisms of earthquakes may vary among regions of the crust. For instance, as a tectonic plate or a crustal block undergoes fracturing and deformation due to mantle impacts, lateral pulling or compression forces may develop between it and adjacent plates or blocks. These continuously increasing lateral pulling or compression forces can also lead to fractures and earthquakes in boundary areas. However, since all these processes originate from mantle impacts that cause localized subsidence of material under the influence of gravity, the corresponding intraplate earthquakes and plate/block boundary earthquakes are related and may even follow the same law.

Regarding the numerous self-organized critical phenomena observed in nature, their essence likely lies in the inherent organizational structure of matter. All matter consists of smaller structures forming larger structures, which in turn compose even larger structures in an organized hierarchy. For this reason, when subjected to external forces, the macroscopic behavior of matter indirectly reveals its internal organizational framework, no matter whatever this process is critical (triggered and autonomously sustained) or non-critical (one-time), nothing but the scale of the displayed organizational structure depends on the mode and intensity of the interactions involved. For example, during a mountain blasting, the size distribution of fractured rock fragments corresponds to the original fine organizational structure of the mountain. However, the range of the displayed structure varies under different TNT equivalents. Similarly, repeatedly hammering a wall will lead to its collapse, and the number and size of the debris fragments will exhibit a clear logarithmic-linear relationship. Yet, using hammers of different sizes or applying different levels of force will result in significant variations in the distribution range of the fragments. This can be understood as each structure having an optimal energy threshold for destruction. The hierarchical organization of matter determines that its absorption of external energy also occurs in a hierarchical manner (i.e. quantized manner). This should be similar to the quantization phenomenon we observe in the microscopic world.

The Earth's crust absorbs energy mainly through two processes—deformation and fracturing—following the cyclic impact of mantle or the continuously increasing static stress. Deformation corresponds to a slow energy absorption process, while fracturing corresponds to a rapid energy absorption process with part of the absorbed energy released by causing earthquakes. The released

energy by earthquakes should include the changes in local gravitation potential that is stimulated by the impact of mantle dynamics. It is proposed, based on the consideration stated above, that earthquakes of different magnitudes correspond to the fracturing of different structural levels within the crust. A magnitude 3 earthquake corresponds to the fracturing of a level-3 structure, a magnitude 4 earthquake corresponds to the fracturing of a level-4 structure, and so on. Since a level-4 structure is composed of multiple level-3 structures, and a level-5 structure is composed of multiple level-4 structures. It means that within the same structural hierarchy the occurrence of multiple magnitude 3 earthquakes will lead to a magnitude 4 earthquake, and the occurrence of multiple magnitude 4 earthquakes will lead to a magnitude 5 earthquake, and so forth. In other words, the occurrence of a large earthquake in a region is the result of the accumulation of a sufficient number of smaller earthquakes, or rather, the destruction of a large structure in the crust is the consequence of the destruction of numerous smaller structures and reaching a critical level. Clearly, a large earthquake originating in this manner does not require extremely high external forces. This is similar to a building composed of many small structures; the gradual damage to these small structures over time eventually leads to the collapse of the entire building. The taller the building is, the greater the vibrations caused by its collapse. However, such a large-scale collapse does not necessarily require significant external stress; the gravitational potential inherent in the building itself is released as its smaller structures are progressively destroyed.

3. Model construction

The occurrence probability of an earthquake in a specified region is a function of two independent variables: the earthquake magnitude i and the occurrence time t. If the magnitude probability density function is $f(i)$ and the time probability density function is $f(t)$, then the occurrence probability density function $\rho(i,t)$ of an earthquake is:

$$\rho(i,t) = f(i) \times f(t) \qquad (1).$$

The cumulative number of earthquakes with magnitudes greater than i and less than i_m (the maximum magnitude achievable in a region) that occur over the time interval from t_0 to t in the area can be expressed as:

$$N = \iint \rho(i,t)didt = \int_{t_0}^{t} f(t)dt \times \int_{i}^{i_m} f(i)di \qquad (2).$$

It is known that N follows the Gutenberg-Richter law [15] of the form $N=10^{a-ib}$ with a and b (called seismic b value) are constants.

Instead of constructing the probability density function of earthquakes, here starting with constructing the crustal structure itself by assuming that a level i+1 crustal structure is composed of 10^b (here b is the seismic b value) level i crustal structures. Under the proposition that the destruction of large structure is a result of cumulative destruction of smaller structures, the number of magnitude i+1 earthquakes n_{i+1} generated by the destruction of level i+1 structure should be 10^{-b} times the number of magnitude i earthquakes n_i produced by the destruction of level i structure. That is $n_{i+1} = 10^{-b} \times n_i$. Thus, the total number of earthquakes with magnitudes equal to and greater than i occurring in a region over a given period can be expressed as:

$$N_i = n_i + n_{i+1} + n_{i+2} + n_{i+3} + \cdots = n_i \times (1 + 10^{-b} + 10^{-2b} + 10^{-3b} + \cdots)$$

$$\approx \frac{n_i}{1-10^{-b}} \quad \text{(for b>0)} \qquad (3).$$

If the number of earthquakes of magnitude i is defined as $n_i = n_{i0} \times 10^{-(i-i_0)b}$, where n_{i0} is the number of earthquakes of magnitude i_0, then:

$$N_i \approx \frac{n_{i0} \times 10^{-(i-i_0)b}}{1-10^{-b}} \qquad (4).$$

Because it is assumed here that earthquake magnitude is linked to the hierarchical structure of the crust, the relationship between the number of earthquakes and their magnitude reflects the spatial distribution of the local crustal structure.

Regarding the temporal characteristics of earthquakes, that is, the relationship between the number of earthquakes and time, it should, according to the perspective of this study, reflect the physical progressive process in which the successive destruction of small crustal structures leads to the failure of a larger structure (i.e., the accumulation of small earthquakes eventually producing a large earthquake). Under external stress interaction, material typically exhibits two main processes of change. The first is a slow deformation process (a slow energy absorption process), which may sometimes gradually strengthen the material's structure by slowly altering it (e.g., the work-hardening process in metals). The second is a rapid fracturing process (a fast energy absorption process), which weakens the material's structure by causing its damage (e.g., the fracture process in materials). For the Earth's crust, which is an intertwined structure of plastic and brittle materials, the mechanisms of structural strengthening and healing remain unclear. For now, we assume that the effect of external forces primarily results in the destruction of the crustal structure, disregarding any potential strengthening and/or healing effects that external forces might induce. This assumption is particularly reasonable during the later stages of accelerated crustal fracturing, as the slow processes of strengthening and healing in the crust would no longer be sufficient to counteract the fast fracturing process. Since the destruction of small structures reduces the overall strength of a local crust, it makes the region more prone to more structural failure under subsequent impacts of the same stress. Therefore, it is reasonable to believe that the structural destruction of crustal regions under interaction of periodic constant stress or continuously increasing static stress would be an accelerating process. This implies that the frequency of small earthquakes will increase over time prior to the occurrence of a large earthquake.

To theoretically describe this increase in the frequency of small earthquakes, a simple approach is to assume that the rate of increase in the number of earthquakes of magnitude i_0, denoted as dn_{i0}/dt, is proportional to the cumulative number of earthquakes of the same magnitude that have already occurred. That is:

$$\frac{dn_{i0}}{dt} = p \times n_{i0} \qquad (5)$$

Here, p represents the relative earthquake occurrence rate of earthquakes of magnitude i_0 in a region during the time interval t to $t+dt$, expressed as $p = (dn_{i0}/n_{i0})/dt$. It is assumed here that p does not change with time and is independent of magnitude. After integration of equation (5), the number of earthquakes of magnitude i_0 occurring from time t_0 to time t is given by:

$$n_{i0} = n_0 \times 10^{p(t-t_0)\times lge} \qquad (6).$$

Where n_0 is the number of earthquakes of magnitude i_0 at $t = t_0$, and $lge \approx 0.4343$. Substituting equation (6) into equation (4), the total number of earthquakes of magnitude i and above in the time period from t_0 to t is then given by:

$$N_i(t) \approx \frac{n_0 \times 10^{[p(t-t_0)\times lge-(i-i_0)b]}}{1-10^{-b}} \qquad (7).$$

Let

$$\frac{n_0 \times 10^{i_0 b}}{1-10^{-b}} = 10^c \qquad (8),$$

then we have

$$N_i(t) \approx 10^{[p(t-t_0)\times lge-ib+c]} \qquad (9).$$

Formulas (7) and (9) reflect the relationship of the earthquake occurrence in a given region with the local crust geologic structure (earthquake magnitude) and the time. Let the exponential term in equation (9), $p(t-t_0) \times lge + c = a$, then:

$$N_i(t) \approx 10^{(a-ib)} \qquad (10).$$

This is the well-known Gutenberg-Richter law (G-R relationship) [15]. It is evident that a is a function of time and is related to the relative earthquake occurrence rate p and the b value. In a given region, since p, b, and c are constants, a will also have a fixed value for a given time interval. If the cumulative number of earthquakes of magnitude i and above at time t_i, i.e. $N_i(t_i)$, is set to 1, then from equation (9):

$$t_i = t_0 + \frac{ib-c}{p\times lge} \qquad (11).$$

This is the time corresponding to the first occurrence of a magnitude i earthquake in the region. If the maximum possible earthquake magnitude in the region is i_m, and the minimum earthquake magnitude i_0 is sufficiently small, then t_i - t_0 in equation (11) approaches the gestation or recurrence period T_m of the largest earthquake in the region, that is,

$$t_{i_m} - t_0 = \frac{i_m b-c}{p\times lge} \approx T_m \qquad (12).$$

It should be noted that, due to the existence of an upper limit on earthquake magnitude in each region, the b value tends to increase in the high-magnitude range. Therefore, when using equation (12) to calculate T_m, the b value should be corrected accordingly.

Using equation (9), the small earthquake data before the largest earthquake in a region can be fitted to obtain the local seismic parameters, including p, c, t_0, and b. These parameters can then be used in equation (11) to calculate the future seismic trends in the region (i.e., to determine the time corresponding to the first occurrence of an earthquake of magnitude i in the region). During fitting, the constant b value for the region (denoted as b_0) can be preliminarily determined using small earthquake data, and set $b = b_0$. At the same time, the c value can be set to zero (i.e., assuming that at $t = t_0$, the cumulative number of earthquakes of magnitude $i_0 = 0$ and above, $N_{i0}(t_0)$, equals to 1, see equations (8) and (9)). This leaves only p and t_0 as the two parameters to be determined during fitting.

It is important to note that when analyzing small earthquake data, the size and location of the selected area should be carefully considered. Apart from not deviating too far from the core area, the area should neither be too small nor too large, If the area is too small or deviates from the core area, the data of small earthquake may be incomplete, making it insufficient to reflect the entire preparation process of a single large earthquake, because the number n_{i0} of earthquakes of magnitude i_0 at any time t should satisfy formula (6). If the area is too large, the data may come from two or more large earthquake-preparation regions, thus exceeding the application scope of the theory. Additionally, the time span of the selected data should be sufficiently long to include enough small earthquake data for fitting. It is also necessary to exclude aftershock data from previous major earthquakes in the area to avoid interference with the fitting process.

In reality, however, it is very hard to know where the epicenter is and how extensive the scope of a large earthquake can be before a large earthquake occurred. It is therefore a practical way to carry out the analysis of earthquake data from area to area by assuming all the selected areas are the independent large earthquake preparation zones, and then make comprehensive analysis by synthesis of information got from different areas. In this way the 3D (location-time-magnitude) problem of the earthquake prediction is simplified into 2D (time-magnitude) problem, which enables the evaluation of future seismic activities from area to area and this certainly helps to locate the position of the preparation zone of a future large earthquake.

The above derivation is based on formula (5). To make the theory more inclusive, we can assume that the number of earthquakes of magnitude i_0 increases with time t at the power of q of the cumulative number of earthquakes of that magnitude, i.e.:

$$\frac{dn_{i0}}{dt} = p \times n_{i0}^{q} \qquad (13).$$

So for q=1 we have eq.(7) and eq.(9). If $q \neq 1$ then we have:

$$n_{i0} = [n_0^{1-q} + (1-q) \times p \times (t-t_0)]^{\frac{1}{1-q}} \qquad (14)\ ,$$

$$N_i(t) \approx \frac{[n_0^{1-q}+(1-q)\times p\times(t-t_0)]^{\frac{1}{1-q}}}{1-10^{-b}} \times 10^{-(i-i_0)b} \qquad (15).$$

Let $\frac{[n_0^{1-q}+(1-q)\times p\times(t-t_0)]^{\frac{1}{1-q}}\times 10^{i_0 b}}{1-10^{-b}} = 10^{a}$, then we have the G-R relationship $N_i(t) \approx 10^{(a-ib)}$. For fitting, i_0 can be fixed to 0 and n_0 to 1, so that the cumulative number of earthquakes of magnitude i_0=0 and above at $t = t_0$, $N_{i0}(t_0)$, equals to $1/(1\text{-}10^{-b})$. In this case, equation (15) is simplified to:

$$N_i(t) \approx \frac{[1+(1-q)\times p\times(t-t_0)]^{\frac{1}{1-q}}}{1-10^{-b}} \times 10^{-ib} = 10^{(a-ib)} \qquad (16).$$

with

$$a = \log\left\{\frac{[1+(1-q)\times p\times(t-t_0)]^{1/(1-q)}}{1-10^{-b}}\right\} \qquad (17).$$

Thus, the time t_i corresponding to the first occurrence of an earthquake of magnitude i in the region (i.e. set $N_i(t_i)$=1) is:

$$t_i = t_0 + \frac{\left[(1-10^{-b})\times 10^{ib}\right]^{1-q}-1}{(1-q)\times p} \qquad (18).$$

The time period T_m for the occurrence of the largest earthquake in the region (with magnitude i_m) is:

$$T_m \approx t_{i_m} - t_0 = \frac{\left[(1-10^{-b})\times 10^{i_m b}\right]^{1-q}-1}{(1-q)\times p} \qquad (19).$$

For q>1, equation (19) shows that T_m will approximately equal to 1/[(q-1)*p] at extremely large earthquake magnitudes.

Similarly, equations (15) and (16) reflect the relationship of the earthquake occurrence in a given region with the local crust geologic structure (manifested by earthquake magnitude) and the time. Using equation (16), small earthquake frequency data prior to a large earthquake in a region can be fitted to obtain the local seismic parameters, such as p, q, and t_0 (the constant b value for the region (denoted as b_0) can be preliminarily determined using small earthquake frequency data). These parameters can then be used in equation (18) to determine the future seismic trends in the region (i.e., to estimate the time corresponding to the first occurrence of an earthquake of magnitude i in the region). Interestingly, with a fixed magnitude i, equation (15) is very similar in form to the Paris model [16] that describes the growth of micro cracks during the fatigue fracture process of metallic materials. The parameter q here is equivalent to m/2 in the Paris model. The Paris model describes the steady growth process of cracks in metal materials under low cyclic stress (requires $2 < m < 4$). The continuous growth of these cracks eventually leads to the fracture of the material. Equating the earthquake magnitude with the unit of crack length and the accumulation of small earthquakes with the growth process of crack length, a similar relationship can be derived.

4. Application and discussion

4.1 Analysis of Earthquake Data in a Region of Sichuan Province, China

Figure 1 shows the spatiotemporal distribution of earthquakes with magnitudes greater than M4 that occurred in a region of Sichuan Province, China, between 1980 and 2024 (data sourced from USGS [17]). Figure 2 illustrates the longitude and latitude distribution of earthquakes in this region (longitude 104.4–106.0, latitude 27.5–30.0, marked as Zone I) during the 45 years. It is evident that a large number of earthquakes with magnitudes of 4 and above are distributed unevenly in time and space. Because it is unclear how many major earthquakes are in preparation in this region, the investigation was conducted not only on the data from the entire region (Zone I) but also on the data from several smaller subregions to examine the impact of area selection on the analysis. These include the red-boxed region (longitude 104.4–105.4, latitude 27.7–29.7, marked as Zone II) and the blue-boxed region (longitude 104.4–105.4, latitude 27.9–28.9, marked as Zone III) in Figure 2, Based on the cumulative earthquake frequency data for magnitudes 4.0+ and 4.5+ in the entire region (Zone I) from 2000 to 2024, the b_0 value (defined as $\log(N_{4+}/N_{4.5+})/0.5$) for this area is selected as 0.73±0.08 (see Figure 3). Therefore, in all subsequent fittings for data from various regions, the b_0 value is fixed at 0.73, and the impact of changes in the b value on the results is analyzed as well.

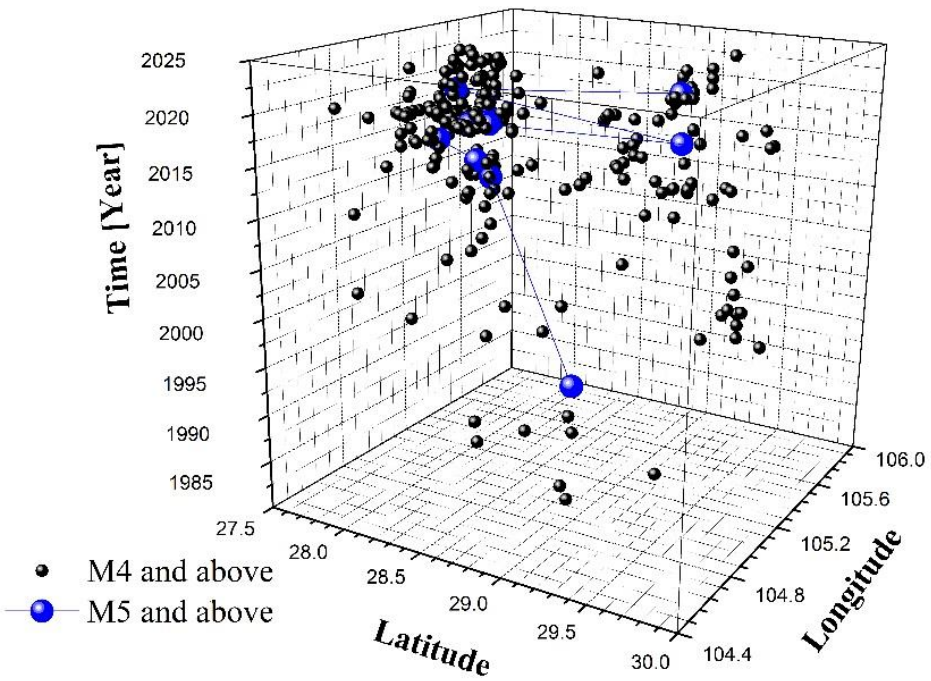

Figure 1. Spatiotemporal distribution of earthquake events in a region of Sichuan Province, China, from 1980 to 2024.

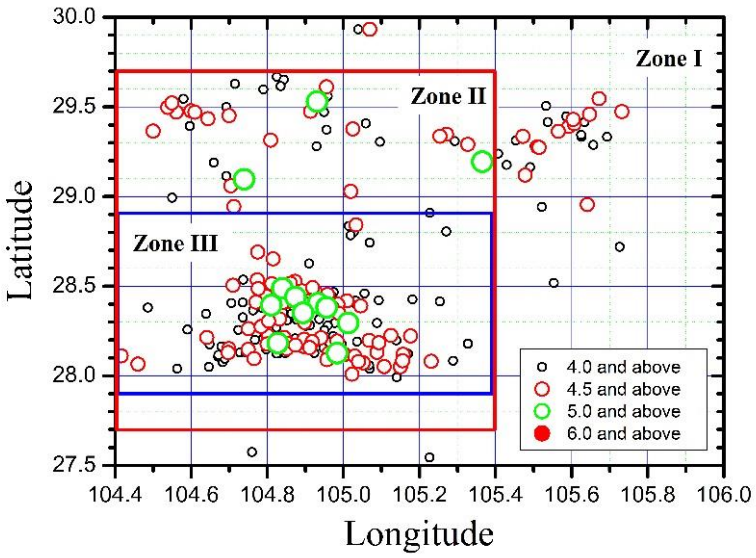

Figure 2. Longitude and latitude distribution of earthquakes in a region of Sichuan Province, China, from 1980 to 2024, and selection of analysis areas.

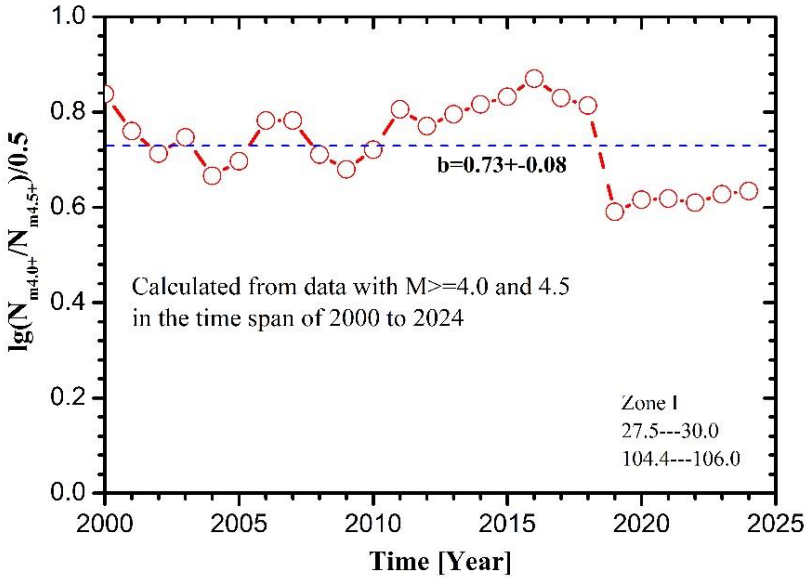

Figure 3. Estimation of the *b*-value for local earthquake data analysis.

Figure 4 illustrates the fitting of cumulative earthquake frequency data for magnitudes of 4.5 and above in Zone I from 1980 to 2024 using equations (9) and (16), respectively, with the *b* value being fixed at 0.73 during fitting. Since the earthquake data in Figure 4 is based on records starting from 1980, the year 1979 is used as the starting point for data fitting. The cumulative earthquake quantity is expressed as the differential $\Delta N_i(t)$ (see equations (20) and (21)), representing the total cumulative number of earthquakes from time t_0 to t minus the cumulative number of earthquakes expected before 1979.

When fitted using equation (9):

$$\Delta N_i(t) = 10^{[p\times(t-t_0)\times lge-ib+c]} - 10^{[p\times(1979-t_0)\times lge-ib+c]} \qquad (20).$$

When fitted using equation (16):

$$\Delta N_i(t) = \left\{[1+(1-q)\times p\times(t-t_0)]^{\frac{1}{1-q}} - [1+(1-q)\times p\times(1979-t_0)]^{\frac{1}{1-q}}\right\}\times\frac{10^{-ib}}{1-10^{-b}} \qquad (21).$$

From Fig.4, it can be observed that both equation (9) and equation (16) can fit the data. In particular, for the period between 2010 and 2024, the two models yield almost identical results. However, significant differences are observed in the results for the data prior to 2010 and the predicted results beyond 2024. For the data prior to 2010, the fitting results from equation (16) align better with the actual data, whereas the predictions beyond 2024 remain to be evaluated by future observations. Table 1 shows the parameters obtained by fitting and compares the changes in fitting parameters for different *b* values.

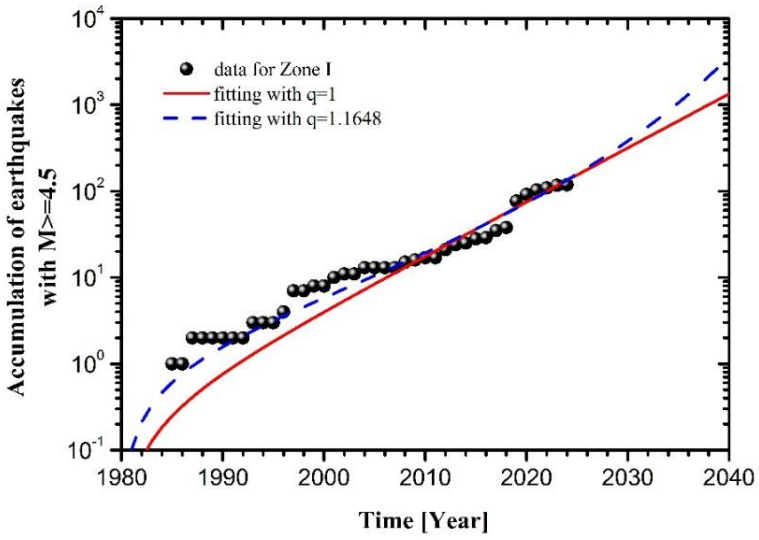

Figure 4. Fitting of earthquake data in Zone I. The solid line is the fitting result obtained using formula (9); the dotted line is the fitting result obtained using formula (16).

Table 1. Comparison of fitting parameters for M4.5+ earthquake data (1980–2024) in Zone I under different b values (with c fixed at 0). Upper part with q=1 are fittings by using eq.(9). Lower part with q≠1 are fittings by using eq.(16).

b value	q	error	p	error	t_0 (year)	error	χ^2	R^2
0.81	1	-	0.14461	0.00735	1932.1	8.7	48.2	0.957
0.73	1	-	0.14421	0.00737	1937.6	8.2	48.2	0.957
0.65	1	-	0.14424	0.00740	1943.4	7.6	48.2	0.957
0.81	1.1532	0.0054	0.02101	0.00256	1754.9	42.2	50.1	0.956
0.73	1.1648	0.0075	0.02097	0.00280	1772.9	41.3	50.3	0.956
0.65	1.1762	0.0109	0.02148	0.00327	1795.3	40.8	50.5	0.955

Figures 5a and 5b illustrate the relationship between the time t_i of the first occurrence of an earthquake and its magnitude i, calculated by using equations (11) and (18) based on the fitting parameters (table 1) obtained under different b values. It can be seen from the figures that the two models (equations (9) and (16)) produce similar predictions for the first occurrence time of earthquakes with magnitudes above 5, but they differ significantly in their predictions for earthquakes with magnitudes below 5. This indicates that the two models exhibit notable differences in describing

the early stages of small earthquakes evolving into large earthquakes. Additionally, as shown in Table 1 and Figure 5, the ±0.08 variation in the b value has little impact on the results under both models. Zoomed-in views (Figures 5c and 5d) reveal that, for different *b* values, the predicted first occurrence times for a magnitude 7 earthquake in this region are approximately 2016 (*b*=0.65), 2019 (*b*=0.73), and 2023 (*b*=0.81), respectively. The rule is that when M≥5, the smaller the *b* value, the higher the magnitude of the earthquake occurred for the first time in the same period. It should be noted that this calculation does not account for the effect of *b* value increase among large-magnitude earthquakes. The adjustments to *b* values for large-magnitude earthquakes will be discussed in subsequent sections.

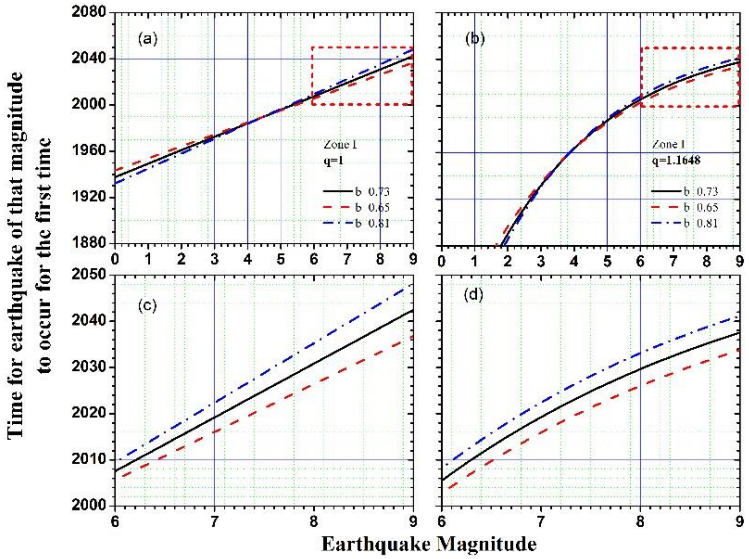

Figure 5. The impact of the *b*-value on earthquake trend predictions. (a) Calculation results for Zone I data using equation (11). (b) Calculation results for Zone I data using equation (18). (c) Magnified view of the red dashed box region in Fig.5(a). (d) Magnified view of the red dashed box region in Fig.5(b).

The left panel of Figure 6 shows the fitting of M4.5+ earthquake data from Zone I over three different periods starting from 1980, 2000, and 2010, respectively, to 2024 using equation (16) to evaluate the impact of data collection periods on the fitting results. Here, only the fitting results from equation (16) are presented, as the conclusions derived from fitting with equation (9) are entirely consistent. The right panel of Figure 6 presents the difference between the theoretical and observed values (i.e., the negative value of the residuals) to indicate the seismic hazard level of the region. That is, when the theoretical value is significantly higher than the actual value, it means that the earthquake accumulation in the local area is insufficient and there is potential for earthquakes to occur; when the theoretical value is significantly lower than the actual value, it means that the local crustal energy has been fully released and the occurring possibility of another earthquake is reduced. As shown in Figure 6, the fittings for the three time intervals yield similar residual values and patterns after 2010, indicating that meaningful results can be obtained even for relatively short datasets (in this case, 15 years span only) as long as the data is sufficiently abundant. As illustrated, the seismic hazard level in the region decreased significantly following a magnitude 5.7 earthquake in 2019, reaching its lowest point in 2020 before rapidly increasing again after 2021. This phenomenon reflects the staged (i.e., quantized) energy absorption nature of crust determined by the hierarchical structural

characteristics of the crust. As shown, the period from the deviation of the 2019 data from the theoretical value to the return of the 2023 data near the theoretical value lasted approximately five years. If the time required for the next jump is also estimated to be around five years (i.e., assuming the theoretical value represents the statistical average of actual data), it suggests that a large earthquake might occur in the period around 2028. This means that the residuals can serve as a rough forecast signal of future earthquake trends, and such forecasts can be revised annually as more earthquake data becomes available. Table 2 presents the fitting parameters for M4.5+ earthquake data in Zone I for the three different time intervals. It can be observed that although the fitting parameters for different time intervals are similar, shorter time interval fitting yield larger parameter uncertainties.

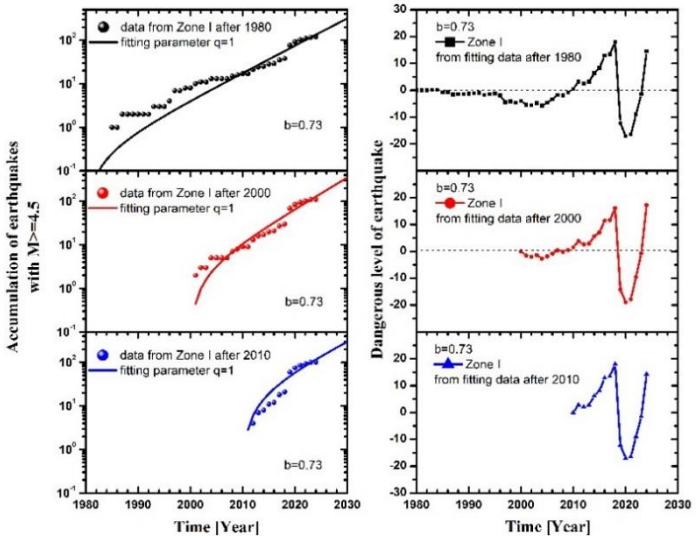

Figure 6. Comparison of earthquake data fitting and residuals for Zone I over different time intervals.

Table 2. Summary of parameters obtained from fitting M4.5+ earthquake data in Zone I over different time intervals (with b=0.73 and c=0 fixed).

Data time span	q	error	p	error	t_0 (year)	error	χ^2	R^2
1980-2024	1.1648	0.0075	0.02097	0.00280	1772.9	41.3	50.3	0.956
2000-2024	1.1681	0.0157	0.02130	0.00626	1780.2	94.8	97.6	0.933
2010-2024	1.1488	0.0910	0.02067	0.03981	1750.7	653.3	155.4	0.905

The above discussion is based on the earthquake data for the entire region (Zone I) shown in Figure 2. If earthquake trend information can be obtained by reducing the area of the analysis region, it will be more helpful to determine the location of future earthquakes. Therefore, the red-framed region (Zone II) and the blue-framed region (Zone III) are selected from Zone I for data analysis (Figure 2), where Zone I covers Zone II and Zone II covers Zone III. Table 3 compares the parameters obtained by fitting the data of earthquakes of magnitude 4.5 and above from 1980 to 2024 for the

three regions. The fittings were performed using equations (9) and (16), respectively. Figure 7 shows the corresponding relationship between the magnitude of the earthquake in the three regions and the time of its first occurrence calculated based on the parameters listed in Table 3. The left side shows the result calculated using formula (11) (Figure 7a) and its local enlargement (Figure 7c), and the right side shows the result calculated using formula (18) (Figure 7b) and its local enlargement (Figure 7d). Overall, the first occurrence times for earthquakes with magnitudes of 6 or greater do not vary significantly across the three regions. Slight differences can be seen after local magnification. For magnitudes below 8 (as the maximum earthquake magnitude in most crustal regions is typically below 8, calculations for M8+ are not discussed here), it can be observed that the larger the selected region, the earlier the first occurrence time for earthquakes of the same magnitude. Specifically, the first occurrence times for M7 earthquakes, as determined from the data for Zones I, II, and III, are 2019.2, 2020.4, and 2021.9, respectively, with differences from each other of 1.2 years and 1.5 years. Figures 7a and 7c are derived from equation (11), which is based on equation (9) with $N_i(t_i)=1$, assuming that there is only one major (possibly the largest in the area) earthquake preparation in the region. However, if it is assumed that Zone I contains two major earthquake preparation points developing in sync (i.e., setting $N_i(t_i)=2$), with one located within Zone II and the other outside of it, then according to equation (9), the difference in the first occurrence times between the two regions would be approximately $\log(2)/0.4343/p \approx 4.1$ years (take p=0.16876, see table 3). Yet, as shown in Figure 7, the difference in the first occurrence times for M7 earthquakes between Zones I and II is only 1.2 years, and the difference between Zones I and III is less than 3 years. This suggests that there is likely only one major earthquake preparation in the area. Alternatively, even if there is another one in preparation, their development periods will not overlap significantly, means that their mutual influence can be ignored.

Table 3. Parameters obtained from fitting M4.5+ earthquake frequency data from 1980 to 2024 in three regions (with b=0.73 and c=0 fixed). Upper part are fittings with q=1 by using eq.(9). Lower part are fittings with q≠1 by using eq.(16).

Zone	q	error	p	error	t_0 (year)	error	χ^2	R^2
I	1	-	0.14421	0.00737	1937.6	8.2	48.2	0.957
II	1	-	0.16876	0.00961	1950.7	8.5	46.1	0.950
III	1	-	0.19245	0.01207	1960.8	8.8	33.4	0.942
I	1.1648	0.0075	0.02097	0.00280	1772.9	41.3	50.3	0.956
II	1.1754	0.0069	0.02165	0.00258	1791.7	36.7	53.9	0.941
III	1.1844	0.0072	0.02273	0.00262	1811.7	34.2	42.0	0.927

Since the first occurrence times for M7 earthquakes determined from the three regions are very close, and the cumulative number of earthquakes within Zone III accounts for more than 70% of the total in Zone I and more than 79% in Zone II, it can be inferred that the major earthquake preparation point for this cycle is likely located within Zone III. That is, if the data from Zone III were excluded, it would not be possible to deduce the occurrence of an M7+ earthquake in the near future for this region. In fact, due to insufficient data remaining after excluding data in Zone III, even the theoretical fitting described in this study could not be performed.

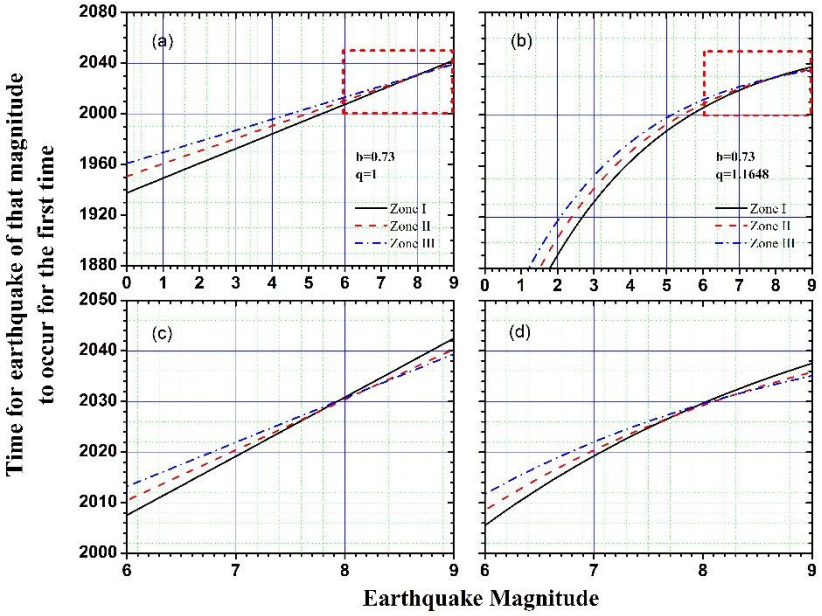

Figure 7. Earthquake trend predictions derived from fitted parameters of earthquake data in different regions. (a) Results calculated by using parameters obtained with equation (9). (b) Results calculated by using parameters obtained with equation (16). (c) Magnified view of Fig.7(a). (d) Magnified view of Fig.7(b).

As mentioned above, the calculation results shown in Figures 5 and 7 do not consider the effect of the increased *b* value occurred at large earthquakes. There is evidence that as the magnitude of earthquakes in each region approaches its limit, the number of earthquakes decreases significantly, which leads to a rapid increase in the *b* value. To reflect this phenomenon, the following relationship between the *b* value and magnitude *i* is proposed:

$$b = b_0 \times (1 + H \times 10^{(i-i_c)/\Delta i}) \qquad (22)\ ,$$

where H, i_c and Δi are variable parameters, and b_0 is the constant b value for low-magnitude earthquakes. The parameters used for correction in this paper are H=0.01, i_c=6.0 and Δi=1.0. It should be noted that the correction here is only a demonstration, not a calculation based on facts. Formula (22) and its parameters should be optimized according to the actual situation in each place. As is well known, the theoretical description of large earthquake behavior near the magnitude limit remains one of the central challenges in this field [6, 18]. This paper only takes formula (22) as an example to illustrate how changes in the *b* value will affect theoretical predictions. Figure 8 shows the changes in the results of Figure 7 after the *b* value is corrected as above. It can be seen from the figure that the

increase in the *b* value leads to a rapid increase in the first occurrence time of large-magnitude earthquakes. As predicted by equation (18), with magnitudes high enough the first occurrence time of earthquakes will approach a constant value (Figures 8b and 8d). Previously, based on the residual trend shown in Figure 6, it was judged that a large earthquake in the studied area might occur around 2028. If the *b* value correction here is reasonable, it indicates that the magnitude of the earthquake occurring around 2028 will be around 7.01 (see Figures 8c and 8d), while the corresponding magnitude of the earthquake without *b* value correction will be around 7.76 (see Figures 7c and 7d).

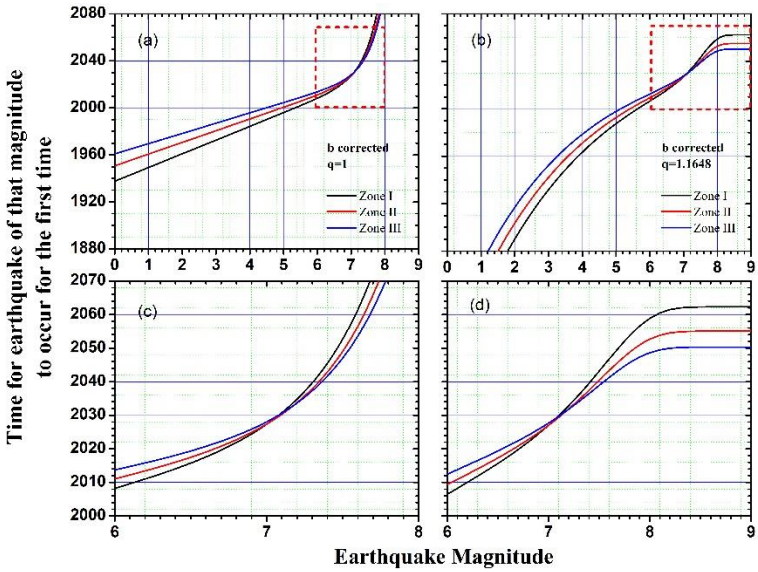

Figure 8. Earthquake trend predictions derived from fitted parameters of earthquake data in different regions (after *b*-value correction). (a) Results calculated by using parameters obtained with equation (9). (b) Results calculated by using parameters obtained with equation (16). (c) Magnified view of Fig.8(a). (d) Magnified view of Fig.8(b).

4.2 Analysis of Earthquake Data in Italy

Figure 9a shows the longitude and latitude distribution of M4+ earthquakes over a 45-year period (1980–2024) across a region covering almost the entirety of Italy (longitude 11–15, latitude 41–45, marked as Zone I), with data sourced from USGS [17]. Figure 9b is a magnified view of the red-boxed area in Figure 9a (longitude 12.5–13.5, latitude 42.0–43.5, marked as Zone II). Figure 10 illustrates the spatiotemporal distribution of M4+ earthquakes in Zone II from 1980 to 2024. From Figures 9 and 10, it is evident that a large number of M4+ earthquakes in the described region are unevenly distributed in both time and space. The reported *b* values across Italy vary widely in the literature, which is related to differences in the geological structures of different areas. In this paper, the temporal variation of $\log(N_{m4+}/N_{m5+})$ was calculated using cumulative data for M4.0+ and M5.0+ earthquakes in Zone I (see Figure 11). The average value from 2013 to 2024 was found to be 1.1 and is used as the fixed *b* value for all subsequent fitting in various regions. Additionally, the impact by taking b=0.9 and b=0.7 on the analysis was also investigated.

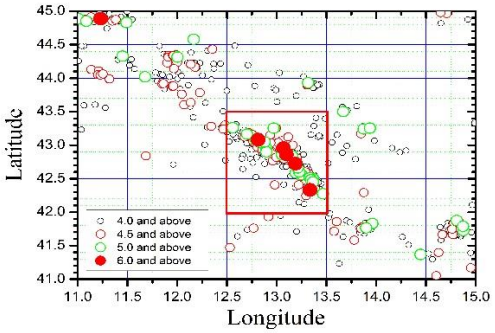

Figure 9a. Longitude and latitude distribution of M4+ earthquakes in Italy and surrounding regions (marked as Zone I) from 1980 to 2024.

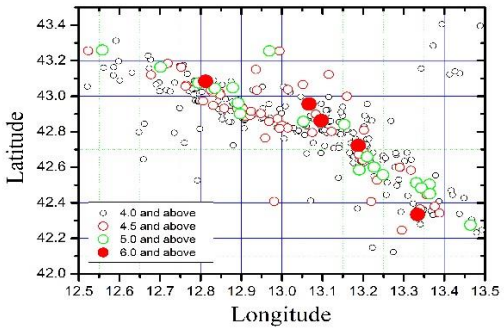

Figure 9b. Longitude and latitude distribution of M4+ earthquakes in the red-boxed region (marked as Zone II) of Figure 9a from 1980 to 2024.

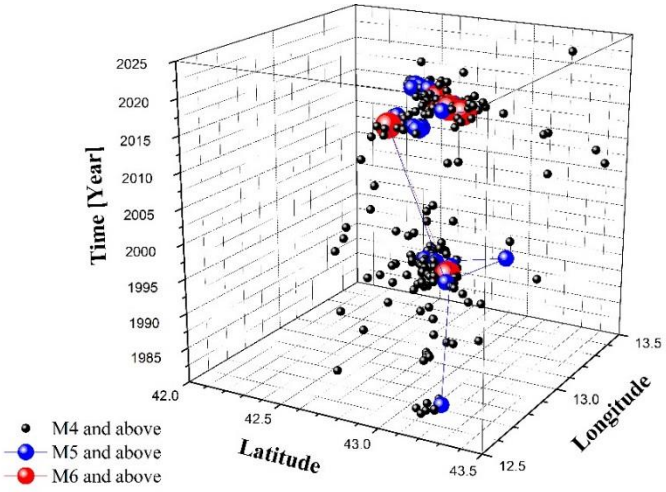

Figure 10. Spatiotemporal distribution of M4+ earthquakes in a local region (Zone II) of Italy from 1980 to 2024.

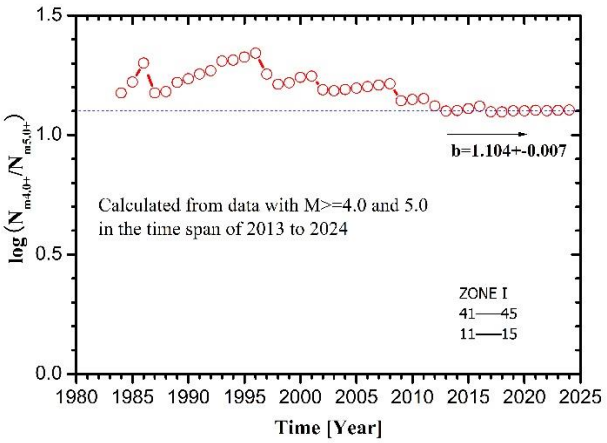

Figure 11. Estimation of the *b* value in the analyzed region.

Figure 12 shows the fitting of cumulative M4.5+ earthquake data in Zone I from 1980 to 2024 using equations (9) and (16), respectively, with b being fixed at 1.1. Since the earthquake data in Figure 12 is based on records starting from 1980, the year 1979 is used as the zero point for the earthquake data fitting. The cumulative earthquake quantity is expressed as the differential $\Delta N_i(t)$ (see equations (20) and (21)), representing the total cumulative number of earthquakes from time t_0 to t minus the cumulative number of earthquakes expected before 1979. From Figure 12, it is clear that both equation (9) and equation (16) can fit the data, and the q value obtained from the fitting with equation (16) is very close to 1. Therefore, only equation (9) is used for subsequent fittings. Table 4 presents the parameters obtained from the fittings and compares the variations of the fitting parameters under different b values.

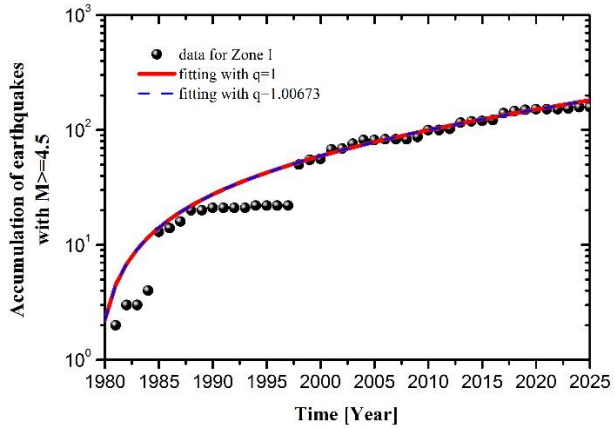

Figure 12. Fitting of earthquake data in Zone I. The solid line is the fitting result obtained using formula (9), and the dotted line is the fitting result obtained using formula (16).

Table 4. Comparison of fitting parameters for M4.5+ earthquake data (1980–2024) in Zone I under different b values (with c=0 fixed). Upper part with q=1 are fittings by using eq.(9). Lower part with q≠1 are fittings by using eq.(16).

b value	q	error	p	error	t_0 (year)	error	χ^2	R^2
1.1	1	-	0.02341	0.00267	1298.2	95.7	74.6	0.975
0.9	1	-	0.02341	0.00270	1386.8	85.2	74.6	0.975
0.7	1	-	0.02341	0.00273	1475.3	74.5	74.6	0.975
1.1	1.00673	0.22131	0.02070	0.18523	1251.7	5331.7	76.4	0.974
0.9	1.00914	0.31830	0.02022	0.18831	1340.1	4725.9	76.5	0.974
0.7	1.01804	0.43377	0.01826	0.17070	1405.4	4180.2	76.5	0.974

Figures 13a and 13b illustrate the relationship between the time t_i of the first occurrence of an earthquake and its magnitude i for Zones I and II, respectively. The calculations are based on the fitting parameters obtained for M4.5+ earthquake data by using equations (11) and (18) under different b values. As can be seen from the figures, the changes on the first occurrence of earthquakes caused by b value variation in the two zones are very similar. Above magnitudes 5, smaller b values correspond to higher first-occurrence magnitude for the same period, and earlier first-occurrence time for the same magnitude. From the magnified views (Figures 13c and 13d), it can be observed that for Zone I, the predicted first occurrence times of M7 earthquakes are approximately 2055.6 (b=1.1), 2006.5 (b=0.9), and 1957.3 (b=0.7), respectively. For Zone II, the predicted first occurrence times of M7 earthquakes are approximately 2084.1 (b=1.1), 2037.9 (b=0.9), and 1991.6 (b=0.7), respectively. These results indicate that the large variation of b value has a significant impact on the prediction of future earthquake trends. It should be noted that these calculations do not account for the effect of b-value increasing associated with high-magnitude earthquakes. If this effect were considered, the corresponding first occurrence times of large earthquakes would be significantly delayed.

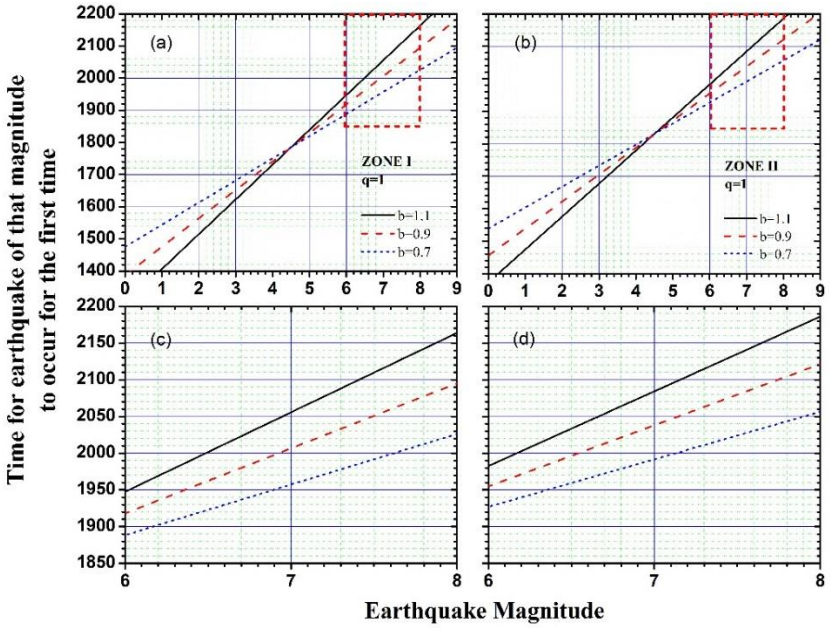

Figure 13. The impact of b values on earthquake trend predictions. (a) Results for Zone I data using equation (11). (b) Results for Zone II data using equation (11). (c) Magnified view of the red dashed box in (a). (d) Magnified view of the red dashed box in (b).

Additionally, as shown in Figure 13, for the same b value, the first occurrence times of large earthquakes predicted for Zone II lag behind those for Zone I by approximately 30 years. This is likely because Zone I covers a larger area than Zone II and may contain 2 or more major earthquake preparation points during the same period, while the results in Figure 13 are calculated by assuming that there is only one major earthquake preparation point within the zone. If it is assumed that Zone II contains only one major earthquake preparation point, while Zone I contains two synchronized major earthquake preparation points (one inside Zone II and another outside), then by using equation (9) with $N_i(t_i)$=2, the first occurrence time of large earthquakes in Zone I would be delayed by approximately log(2)/0.4343/p=29.6 years (with p=0.02341, see table 4) compared to the calculation

with $N_i(t_i)$=1. This result matches the findings shown in Figure 13. Figure 14 presents the earthquake trend predictions for Zones I and II under b=1.1 and b=0.9, respectively, along with the corrected results assuming that Zone I contains two synchronized major earthquake preparation points during the same period. As shown in the figure, after correction, the results for Zone I align closely with those for Zone II (see the magnified views in Figures 14c and 14d), supporting the hypothesis that there are likely two major earthquake preparation points in a large area of Italy during the same period, with one of them located within Zone II. As for whether there is only one major earthquake preparation point in Region II during the same period requires dividing Zone II into smaller subregions for data analysis.

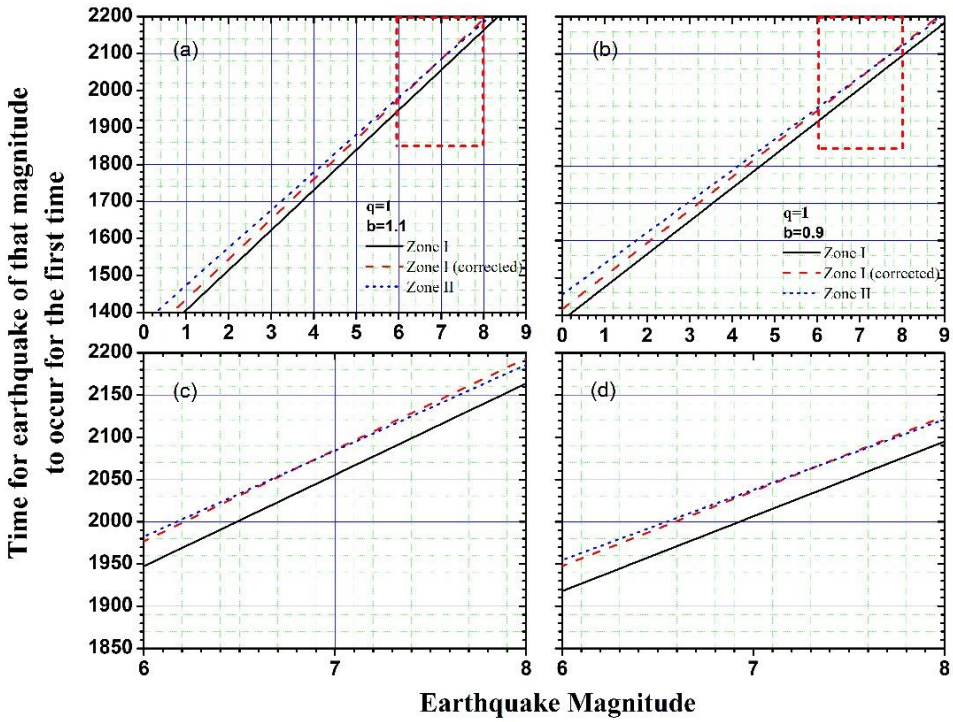

Figure 14. Comparison of earthquake trends between Zone I (solid line) and Zone II (dotted line). (a) Calculations based on parameters fitted with b=1.1. (b) Calculations based on parameters fitted with b=0.9. (c) Magnified view of the red-boxed region in (a). (d) Magnified view of the red-boxed region in (b). The dashed line represents the corrected results for Zone I (solid line) under the assumption that two synchronized large earthquake preparation points exist within Zone I.

Table 5 provides a comparison of the parameters obtained by fitting cumulative M4.5+ earthquake data from 1980 to 2024 in Zones I and II under different b values. The left panel of Figure 15 shows the fitting of cumulative M4.5+ earthquake data for Zones I and II from 1980 to 2024 using equation (20) (with b=1.1 fixed). The right panel presents the difference between the theoretical fitting values and the observed values (i.e., the negative of the residuals), which are used to indicate the local seismic hazard level. As can be seen from Figure 15, the negative value of the residual well reflects the historical events of large earthquakes in the two regions at various stages, indicating that a high negative value of the residual indicates an increased risk of a strong earthquake and can be

used as precursor data. After 2017, the negative values of the residuals in the two zones continued to increase, and by 2024, they had reached a level where an earthquake with a magnitude of 6 or greater could occur again, indicating that preparation for earthquake disaster prevention and reduction need to be made in Zone I, both inside and outside Zone II, in recent years.

Table 5. Comparison of parameters obtained from fitting the earthquake data of magnitude 4.5+ in Zone I and Zone II (with c=0 fixed)

Zone	b	q	p	error	t_0 (year)	error	χ^2	R^2
I	1.1	1	0.02341	0.00267	1298.2	95.7	74.6	0.975
II	1.1	1	0.02490	0.00449	1372.1	136.5	49.2	0.935
I	0.9	1	0.02341	0.00270	1386.8	85.2	74.6	0.975
II	0.9	1	0.02490	0.00453	1455.3	120.7	49.2	0.935

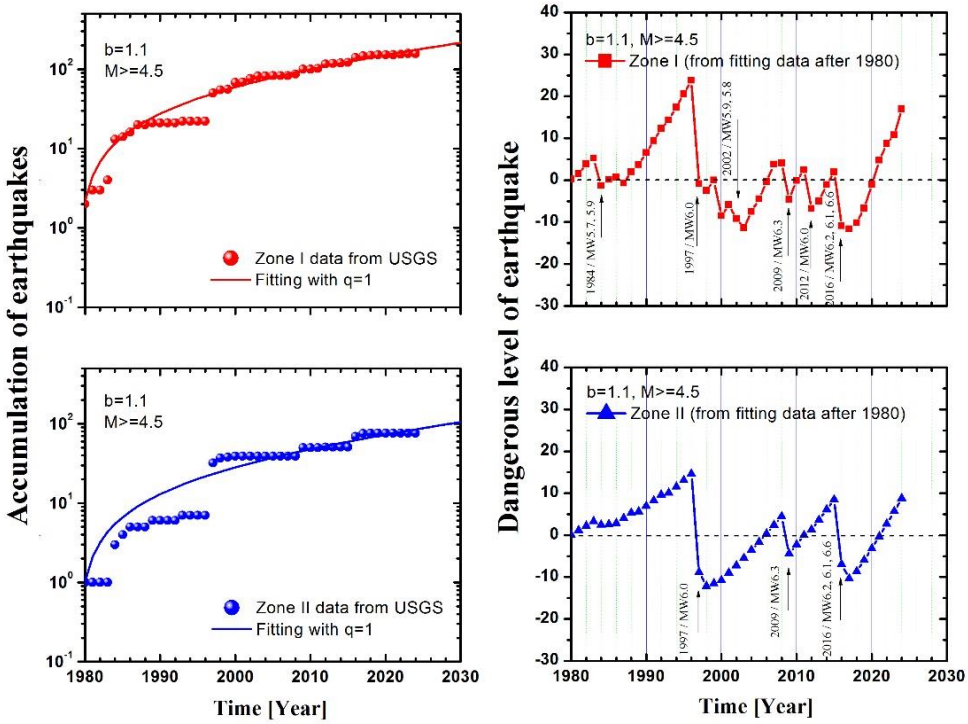

Figure 15. Comparison of the fitting (left) and negative residual values (right) of the cumulative earthquake data in Zone I (top) and Zone II (bottom). The dangerous level of earthquake is defined as the negative value of the fitting residual.

4.3 Discussion

Stress interaction induces fracture of crust and therefore generating earthquakes. Large fractures lead to large earthquakes, and small fractures lead to small earthquakes. Although the accumulation of small fractures is not a necessary condition for the formation of large fractures, it does create the favorable conditions for the formation of large fractures and is certainly an important way to form large fractures. Not only the continuously increasing static stress can produce small fractures, the

Earth's structure and its periodic motion create the condition for the crust to be periodically impacted by fluidic mantle and therefore also induce small fractures. The accumulation of small fractures together with possible superposition of local gravity leads to large fracturing of the crust. This makes it possible to monitor the formation of a large earthquake by observing the accumulation of small earthquakes. The fact that small fractures must accumulate to a certain level before a large fracture can form suggests that there is an effective interaction distance between fractures; the accumulation of small earthquakes that are too far apart are not in favor of the formation of large earthquakes. Areas where the tectonic structure is conductive to stress concentration are more likely to generate closely spaced small earthquakes, and therefore are likely to become the preparation points for a large earthquake.

As mentioned previously, under stress interaction, the Earth's crust absorbs energy not only through crust fracturing. It can also absorb energy through crust deformation, a process of slow energy absorption. If large fracturing (earthquake) of crust is mainly caused by energy accumulation through this slow deformation processes, then the proposed model will not be applicable because very few or even no small earthquakes can be detected before the large event occurred. The process dominating the energy absorption of earth's crust depends on the local geological structure of a region.

Taking the rate of increase in the number of earthquakes over time t being proportional to the q-th power of the cumulative number of earthquakes (equation 13) may be the simplest way to describe the behavior of small fractures evolving into large fractures. The q value obtained from fitting appears to serve as an indicator of different stages in earthquake evolution. When $q \geq 1$, it may indicate that earthquake preparation has matured and entered an accelerated growth phase, while $0 < q < 1$ may suggest that the large earthquake is still in its early developmental stage, whereas $q = 0$ means that there are not yet any interactions (or correlation) between small fractures or that the local energy absorption process of crust is dominated by crust deformation instead of fracturing. At $q > 1$, the relationship between the accumulation of earthquake numbers and time resembles the Paris model [16], which describes the growth of microcrack lengths during the fatigue fracture process of metallic materials. This similarity suggests that the formation mechanism of large earthquakes is analogous to the microscopic fracture mechanism during the final stage of fatigue fracture in metallic materials under low cyclic stress. Metals, due to their excellent microscopic damage recovery mechanisms, only exhibit this damage acceleration phenomenon in the late stages of fatigue. It is expected that crustal materials, with their weaker damage recovery mechanisms, should enter this damage acceleration phase at a much earlier stage.

The discontinuity (jumping nature) in earthquake energy release of local crust provides a potential tool for earthquake prediction. The difference between theoretical predictions and actual earthquake occurrences (negative residuals) can be used to assess seismic hazard levels in different regions. The accuracy of theoretical fitting improves as the amount of earthquake data increases annually, providing a natural basis for continues refining future seismic hazard assessments. The reliability of theoretical calculations depends on the quantity and quality of earthquake frequency data. Sufficient, high-quality earthquake data and a reasonable b-value as well as its correction for large-magnitude earthquakes are critical for obtaining reliable physics predictions.

5. Summary

Based on the Earth's structure and its rotational and orbital dynamics, it is proposed that earthquakes may be a stepwise fracturing process of the crust under the impact of fluid mantle recurring annually together with the interaction of gravity. Using the logarithmic linear relationship between earthquake frequency and magnitude, a structural system of the crust is constructed, wherein smaller structures form larger ones and larger structures form even larger ones. Since the accumulation of small fractures (small earthquakes) in the crust is one of the many ways for the formation of large fractures (large earthquakes), a temporal variation model in the accumulation number of small earthquakes is derived by assuming that the rate of earthquake accumulation is proportional to the q-th power of the existing number of earthquakes. Earthquake data from selected regions of China and Italy are fitted by the theory and the obtained fitting parameters are used to calculate the future trends in seismic activity in these regions. It is found that data analysis by the model from region to region simplified the 3D (space-time-magnitude) problem into 2D (time-magnitude) problem in earthquake prediction and can provide meaningful evaluation of local seismic activity. Deviation of earthquake accumulation from the theoretical expectation can be used as a reasonable judgement of the local seismic dangerous level and $q \geq 1$ can be considered a marker of local crust entering an accelerated fracturing phase. It is believed that reliable physics predictions can be conducted by the proposed model if sufficient high-quality earthquake data and reasonable b-value as well as its correction for large-magnitude earthquakes are available.

References

[1] Utsu T., A list of deadly earthquakes in the world: 1500-2000., In: International handbook of earthquake and engineering seismology, Part A, San Diego: Academic Press, 2002,691-717

[2] Engdahl E.R., Villasenor A., Global seismicity: 1900-1999, In: International handbook of earthquake and engineering seismology, Part A, San Diego: Academic Press, 2002,665-690

[3] Keilis-Borok V. I., Soloviev A.A. (Eds.), Nonlinear dynamics of the lithosphere and earthquake prediction, Springer-Verlag Berlin Heidelberg 2003, ISSN 0172-7389, ISBN 978-3-642-07806-4

[4] Jordan T. H., Operational earthquake forecasting---State of knowledge and guidelines for utilization, **Annals of Geophysics**, 54(4)(2011)316-384 and references therein

[5] Ullah Sh., Bindi D., Pilz M., Danciu L., Weatherill G., Zuccolo E., Ischuk A., Mikhailova N. N., Abdrakhmatov K., Parolai S., Probabilistic seismic hazard assessment for central Asia, **Annals of Geophysics**, 58(1)(2015)S0103; doi: 10.4401/ag-6687

[6] Main I., Statistical Physics, Seismogensis, and Seismic Hazard, **Reviews of Geophysics**, 34(4)(1996)433-462 and references therein.

[7] Geller R.J., Jackson D.D., Kagan Y.Y., Mulargia F., Earthquakes cannot be predicted, **Science**, 275(14)(1997)1616-1617 and references therein

[8] Wyss M., Cannot earthquakes be predicted? **Science**, 278(17)(1997)487 and references therein

[9] Aceves R. L., Park S. K., **Science** 278(17)(1997)488 and references therein

[10] Geller R.J., Jackson D.D., Kagan Y.Y., Mulargia F., **Science**, 278(17)(1997)488-489 and references therein

[11] Kangan Y.Y., Are earthquakes predictable? **Geophys. J. Int.**, 131(1997)505-525 and references therein

[12] Sykes L.R., Shaw B.E., Scholz C.H., Rethinking earthquake prediction, **Pageoph.**, 155(2)(1999)207-232

[13] Reid H. F., The mechanics of the earthquake, The California earthquake of April 18, 1906, Report of the State Investigation Commission, Vol.2, Carnegie Institute of Washington, Washington, D. C. 1910

[14] Kerr R. A., Earth's inner core is running a tad faster than the rest of the planet, https://www.science.org/doi/10.1126/science.309.5739.1313a, **Science**, 309(5739) (2005) 1313

[15] Gutenberg, Richter, Magnitude and energy of earthquake, **Ann Geofis**, 1956, 9:1-15. Republished in: **Annals of Geophysics**, 53(1)(2010)7-12, doi:10.4401/ag-4588

[16] Paris, P.C., Gomez M.P., Anderson W.P., 1961, "A rational analytic theory of fatigue," **The Trend in Engineering**, Vol. 13, pp. 9-14.

[17] http://earthquake.usgs.gov/earthquakes/search

[18] Isabel Serra & Álvaro Corral, Deviation from power law of the global seismic moment distribution, **Scientific Reports**, 2017 | 7:40045 | DOI: 10.1038/srep40045